

Feature-Based Non-Rigid Registration of Serial Section Images by Blending Rigid Transformations

Takehiro Kajihara Takuya Funatomi Hiroyuki Kubo
Graduate School of Information Science
Nara Institute of Science and Technology
Ikoma, Nara, 630-0192, Japan
{kajihara.takehiro.kj7, funatomi, hkubo}@is.naist.jp

Haruyuki Makishima Shigehito Yamada
Graduate School of Medicine
Kyoto University
Sakyo-ku, Kyoto, 606-8501, Japan
{maxima, shyamada}@cac.med.kyoto-u.ac.jp

Takahito Aoto
National Institute of Informatics
Chiyoda-ku, Tokyo, 101-8430, Japan
aoto@nii.ac.jp

Yasuhiro Mukaigawa
Graduate School of Information Science
Nara Institute of Science and Technology
Ikoma, Nara, 630-0192, Japan
mukaigawa@is.naist.jp

Abstract—In this paper, we describe feature-based non-rigid registration of histological serial section images. Our method represents non-rigid deformation by blending the rigid transformations estimated in the local region around a control point. This approach can efficiently represent non-rigid deformation with a smaller number of control points than conventional methods that interpolate displacement, such as free-form deformation (FFD). A feature-based approach is adopted to extract the control points and robustly estimate the local rigid transformation at each control point. By blending the rigid transformations, the displacement at each pixel is computed as a transformation field. The experimental results demonstrate that the proposed method is effective for achieving non-rigid registration efficiently and robustly for histological serial section images.

Keywords—Image registration; Non-rigid deformation; Blending of transformation;

I. INTRODUCTION

Understanding the three-dimensional (3D) structure of biological tissue is crucial for gaining structural insights for physiology and pathology. Histological section images have a much higher resolution compared with MR and CT images. Therefore, a 3D model reconstructed from histological section images provides more detailed structural information. However, histological section images have a non-rigid deformation, such as stretching, bending, folding, and tearing caused by sectioning operations.

For non-rigid registration, free-form deformation (FFD), which is an area-based approach, is popular. Several registration methods for histological images [2], [13] are based on FFD with B-spline interpolation. FFD estimates the displacement at control points and calculates the displacement at every point using interpolation. However, the descriptive power of the deformation highly depends on the resolution of the grid of the control points [10]. A large number of

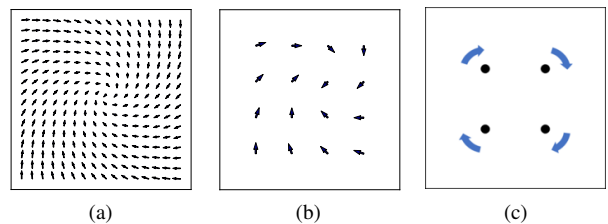


Figure 1. Representation of deformation: (a) displacement in each pixel, (b) displacement field of FFD, where the arrows indicate displacement, (c) transformation field of the proposed method, where the dots indicate the control points and the arrows indicate rigid transformation.

control points are required to represent complex non-rigid deformation.

The feature-based approach is also popular for the global registration technique, such as the rigid or affine transformation of the entire image. The feature-based approach uses invariant local image features for robust matching, and there have been many studies of it in the image processing field [6], [12]. Some feature descriptors have been proposed to be invariant to rotation, translation, and brightness variance, which also occur in histological section images. Although using the local image feature is one of the standard approaches to performing global rigid and affine registration, there is still no standard approach for non-rigid registration. For example, it is not directly applied to FFD because it does not provide the control points on a regular grid.

In histological images, deformations are globally non-rigid, but several studies [4], [3] have been based on the observation that they can be considered to be locally rigid; we also consider this assumption. The contribution of this paper is twofold. First, we present a method that uses a feature-based approach to estimate such local rigid trans-

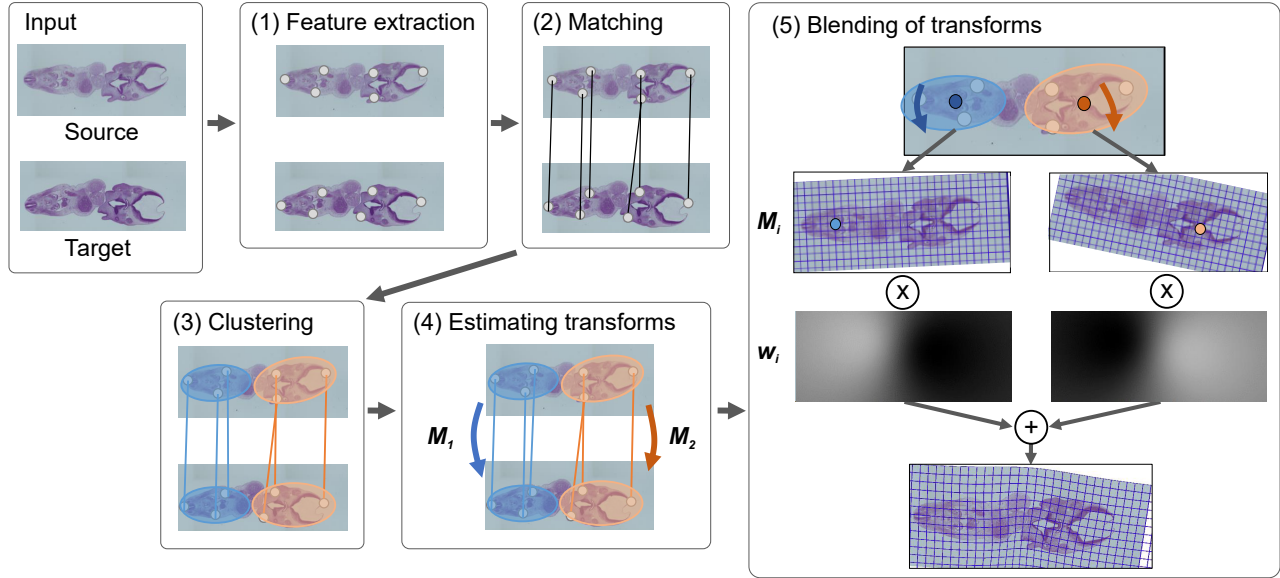


Figure 2. Overview of non-rigid registration for the proposed method: Using source and target images as input, the method (1) extracts feature keypoints, (2) matches them, (3) conducts clustering of the matching (the case for $k = 2$ is shown), and (4) estimates the rigid transformation M_i in each cluster. The transformation field is computed by (5) blending the transformations M_i with weight w_i to represent non-rigid deformation.

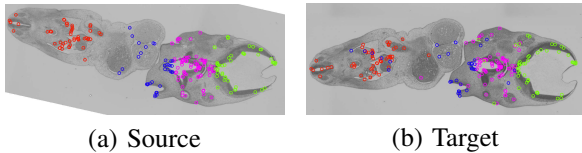


Figure 3. Visualization of clustered keypoints: (a) the transformed source image and (b) the target image. Keypoints in the same cluster have the same color (cluster number $k = 4$). Section images are shown in gray-scale.

formations and integrate them into global non-rigid deformation. To represent a globally non-rigid deformation, we adopt a blending method for rigid transformations. Second, we show that the proposed method efficiently represents non-rigid deformation with a small number of control points as accurately as the FFD approach with a large number of control points.

The proposed method can be considered to extend the FFD approach in two main aspects. First, the control points are defined not on a grid, but on several local regions according to the pattern on the image. We propose an approach to estimate the local regions by clustering the feature points. Second, each control point has a rigid transformation (translation and rotation) where a control point of FFD has a displacement (translation). We call these transformations at every point the ‘*transformation field*’. Because each point has an individual rigid transformation, the transformation field can describe non-rigid deformation on the entire image. For example, if an image has a rotational transformation, as shown in Fig. 1(a), it forms a complex displacement field. FFD represents the deformation using control points

defined on a grid that have a displacement (translation), as shown in Fig. 1(b). The estimated transformation becomes coarse without using a high-resolution grid of the control points. Thus, dense control points are required to represent rotation more accurately. By contrast, the control points of our method have a rigid transformation (translation and rotation), as shown in Fig. 1(c). Therefore, the proposed method can describe complex non-rigid deformation using a smaller number of control points than FFD.

Several methods have been proposed to estimate a transformation at each point from the transformations at the control points. One is the direct average method [11], which is also known as linear blend skinning (LBS) in the computer graphics field. LBS represents rigid transformation M_i in matrix form, takes the weighted sum for each element, and normalizes the resultant matrix so that it represents a rigid transformation. LBS is simple and computationally efficient, but has some artifacts. To reduce the artifacts of LBS, blending using dual quaternion has been proposed in the 3D computer graphics field [7]. The other method is the polyrigid transformation model [4], [3]. The authors used ordinary differential equations (ODEs) to integrate the velocity vector at each control point to obtain the transformations. This method has some mathematically good attributes, such as the invertibility of the resultant transformations. However, these studies did not provide quantitative results that demonstrate the effectiveness of the real-world problem, for example, the registration of histological section images and artifacts of the method are not known. The deformation that occurred in the histological section images would not be limited to

invertible transformations. Therefore, in this study, we use the direct average method with the improvement of reducing the artifacts of blending in two-dimensional (2D) images. This study shows that the transformation field approach is effective for the registration of histological section images, and non-rigid deformation can be modeled using our method.

II. PROPOSED METHOD

The proposed method consists of five steps, as shown in Fig. 2. First, we extract the feature points for the images to be processed and calculate the matching of these points. Next, we define local regions, each of which has rigid deformation, and then estimate a rigid transformation in each cluster. Finally, we compute a transformation field. The following sections explain these steps in detail.

A. Keypoint Detection and Feature Matching

The proposed method estimates rigid transformations based on keypoint detection and feature matching in the same manner as previous methods of rigid registration. Although any method can be used for keypoint detection and feature description, we adopt accelerated-KAZE (AKAZE) [1]. We use AKAZE in OpenCV with the default parameters. By applying the method for the source and target images, two sets of keypoints are acquired (Fig. 2 (1)). Between them, feature matching is performed by brute-force matching using the Hamming distance (Fig. 2 (2)).

To prune improper matching in the background region, the method also extracts the tissue region and removes the matches outside the region. The tissue region is extracted as follows: First, the image is converted to a binary image using the threshold of the UV component in YUV color space. Then we locate the contour of the binary image. Finally, the outside of the contour is masked.

B. Global Registration before Non-Rigid Registration

In addition to non-rigid deformation, the images are affected by the global transformation of rotation and translation, which occurred in the capturing process. The differences caused by such a rigid transformation need to be preliminary eliminated; thus, the algorithm first estimates the rigid transformation between the source and target images using the entire set of matched feature points. The rigid transformation matrix \mathbf{R} is estimated using the Random Sample Consensus (RANSAC) algorithm [5] in the same manner as existing methods. Position \mathbf{p}^s of a pixel on the source image is transformed into $\mathbf{p}^{s'}$ by

$$\mathbf{p}^{s'} = \mathbf{R}\mathbf{p}^s. \quad (1)$$

\mathbf{p}^s and $\mathbf{p}^{s'}$ are homogeneous coordinates.

C. Keypoint Clustering and Estimating Local Transformations

As discussed above, even if the deformation is globally non-rigid, there is a rigid transformation in each local region. Such a local transformation can be estimated from the keypoints in a neighborhood. Thus, we perform k -means clustering for the keypoints on the source image using their coordinates to determine each local region (Fig. 2 (3)). We discuss how to determine the number of clusters k through experiments in Section IV. Using the keypoints in each cluster, a rigid transformation in each cluster \mathbf{M}_i is estimated using RANSAC, as well as the Section II-B (Fig. 2 (4)). Then, we define a control point \mathbf{v}_i as the center of the keypoints used to estimate \mathbf{M}_i in the source image.

D. Calculating the Transformation Field by Blending the Local Rigid Transformations

The proposed method estimates a transformation field that has a rigid transformation at each pixel by blending the rigid transformations $\{\mathbf{M}_i\}$ (Fig. 2 (5)). Blending rigid transformations has been studied in the computer graphics field, and LBS is the most simple method. However, several artifacts occur, such as the candy wrapper effect in LBS. Regarding blending 3D transformations, dual quaternion linear blending (DLB) and dual quaternion iterative blending (DIB) are proposed to overcome the artifact [7]. DIB is mathematically ideal, but requires an iterative process because it is not defined in closed form. For the 2D case, the anti-commutative dual complex and its application to DLB have been proposed [8]. Because the DIB is mathematically preferable, we extend it to the 2D case as dual complex iterative blending (DCIB). The proposed method transforms pixel $\mathbf{p}^{s'}$ in the source image into $\mathbf{p}^{s''}$ using the following:

$$\mathbf{p}^{s''} = \mathcal{F}(\mathbf{w}(\mathbf{p}^{s'}), \mathbf{M})\mathbf{p}^{s'}, \quad (2)$$

$$\mathbf{w}(\mathbf{p}^{s'}) = [w_1(\mathbf{p}^{s'}), \dots, w_k(\mathbf{p}^{s'})]^\top, \quad (3)$$

$$\mathbf{M} = [\mathbf{M}_1, \dots, \mathbf{M}_k]^\top, \quad (4)$$

where k is the number of clusters, $w_i \in [1, k]$ are the blending weights, $\mathbf{M}_i \in [1, k]$ are the rigid transformations of the local regions, and \mathcal{F} is a function of blending the transformations using DCIB.

We empirically set weight w_i at pixel \mathbf{p} according to the Euclidean distance from \mathbf{p} to control point \mathbf{v}_i as follows:

$$t_i(\mathbf{p}) = \frac{1}{\|\mathbf{p} - \mathbf{v}_i\|_2^2}, \quad (5)$$

$$w_i(\mathbf{p}) = \frac{t_i(\mathbf{p})}{\sum_j t_j(\mathbf{p})}. \quad (6)$$

Because the weights need to be convex ($w_i \geq 0, \sum_i w_i = 1$), we normalize the weights to meet the conditions to guarantee the convergence of DCIB. Each pixel has a different rigid transformation because each pixel has an individual

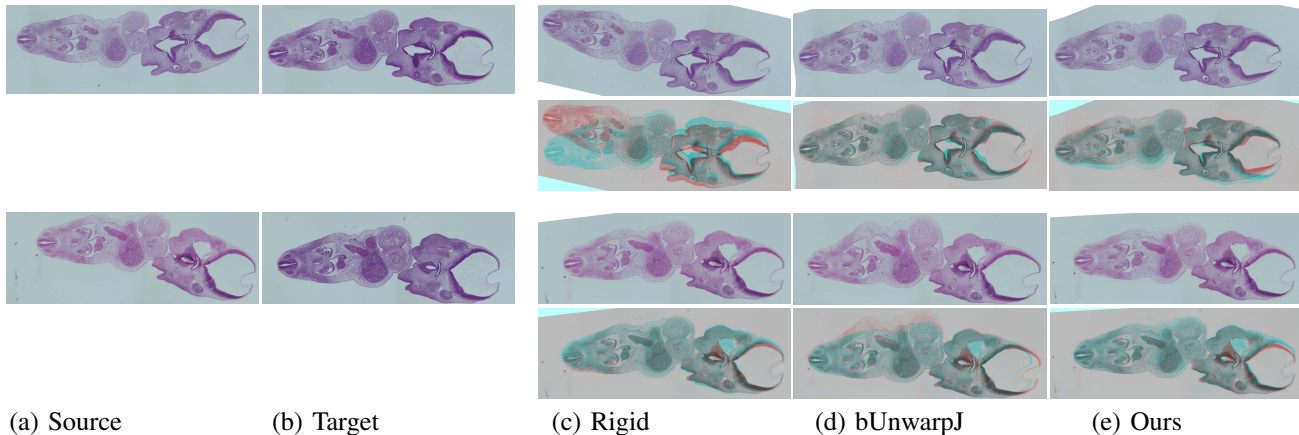


Figure 4. Registration of histological section images: (a) source image, (b) target image, (c) rigid registration, (d) non-rigid registration using bUnwarpJ (deformation grid = 8×8), (e) proposed non-rigid registration (cluster number $k = 8$). We show the images with low staining variation (in the first and second rows) and high staining variation (in the third and fourth rows). The first and third rows show the registration images. The second and fourth rows show the target image in blue and each registration result in red.

weight. Thus, the transformation field represents non-rigid deformation in the entire image, as shown in Fig. 2 (5).

III. EXPERIMENT

We experimentally demonstrated that the proposed method is applicable to the non-rigid registration of a histological section image. For this purpose, we used part of the Kyoto Collection of Human Embryos images maintained in the Congenital Anomaly Research Center, Kyoto University [14]. This study was approved by the Ethics Committee of the Graduate School of Medicine and Faculty of Medicine, Kyoto University (approval nos. R0316 and R0347). The serial sections were approximately 10 micrometers thick, and microscopy was used to capture the images with approximately 5 micrometers resolution. For the evaluation, we selected four specimens from the collection and randomly selected 20 pairs of two neighboring images from each specimen.

We compared our method with one of the existing non-rigid registration methods, bUnwarpJ (elastic registration using B-spline) [2]. Fig. 4 shows the source image (Fig. 4(a)), target image (Fig. 4(b)), and results of registration (Fig. 4(c)–(e)). Because the histological sections were stained chemically, a variation in staining could occur. We show the results of samples with low (the first row) and high (the third row) variations of staining. The second and fourth rows show the overlay of the registration result and target image. The number of the control points for bUnwarpJ was set to 8×8 and the cluster number (k) was 8 for the proposed method. Even though the number of control points used in our method was much fewer than those in bUnwarpJ, the proposed method achieved better performance for samples with high staining variation where bUnwarpJ had a large deformation error, as shown in the bottom row of Fig. 4.

Next, we compared the registration methods in various settings to investigate the effect of the number of control points. We evaluated the registration accuracy using the Jaccard Index (JI) [9]. JI represents the overlap ratio of tissue regions, which was extracted using the method described in Section II-A in two corresponding images as follows:

$$J_{A,B} = \frac{|A \cap B|}{|A \cup B|}, \quad (7)$$

where A and B are the same pixels in the source and target images. The accuracy with various settings is presented in Fig. 5. bUnwarpJ achieved better accuracy with many control points (8×8), and the performance varied together with the number of control points. The proposed method achieved almost the same accuracy with a much smaller number of control points, and performance was relatively stable for the number of control points.

Fig. 6 shows the direct comparison of bUnwarpJ and our method using the same number of control points. Each point represents the JIs for bUnwarpJ and our method for the same pair of sections. If the accuracy was the same, the point was plotted on the diagonal line. The points in the upper left side indicate that the proposed method achieved a better JI than bUnwarpJ. We observe that our method achieved similar or much better accuracy than bUnwarpJ in most samples.

IV. DISCUSSION ON THE NUMBER OF CLUSTERS

Although the proposed method achieved relatively stable performance for the number of clusters, the appropriate number of clusters depends on the deformation that occurred in an image pair. In this section, we present two methods to determine the number of clusters automatically, and compare them to discuss performance.

The first method uses keypoint matches as a criterion to evaluate the number of clusters. For a given number of

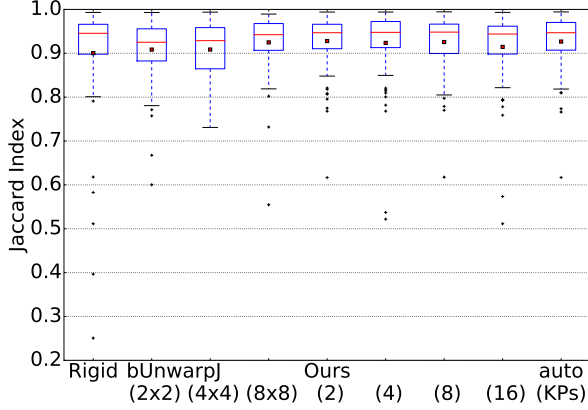


Figure 5. Accuracy of registration using JI: JI of the registration images in each method, rigid registration (Rigid), bUnwarpl and our method (Ours) in various settings. In bUnwarpl, $(n \times n)$ represents the number of deformation grids. In our method, (k) represents the number of control points. Auto (KPs) represents the method for determining number of clusters k using keypoints. Red dots represent the mean.

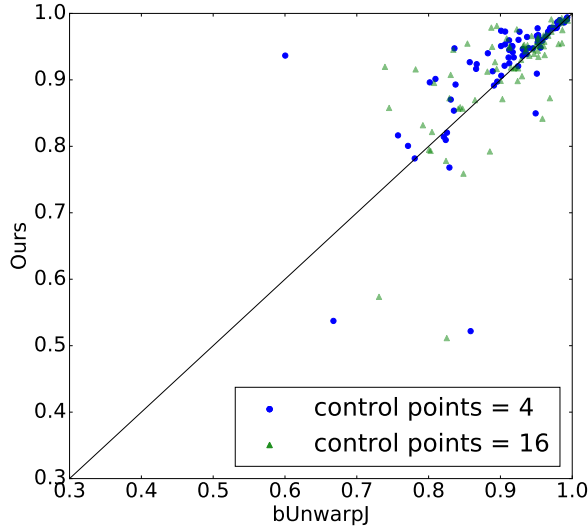


Figure 6. Accuracy comparison of bUnwarpl and our method with the same number of control points for the same image pair. The x -axis shows that the JI of bUnwarpl with deformation grid intervals was $2 \times 2 = 4$ or $4 \times 4 = 16$. The y -axis shows that the JI of our method with control points was 4 or 16.

clusters k , a transformation field was computed using the proposed method. We evaluated it using error e_k defined on keypoint matches calculated as follows:

$$e_k = \sum_{(\mathbf{p}^{s'}, \mathbf{p}^t)} \left(\mathbf{p}^t - \mathcal{F}(\mathbf{w}(\mathbf{p}^{s'}), \mathbf{M}) \mathbf{p}^{s'} \right), \quad (8)$$

where \mathbf{p}^t is a keypoint in the target image that corresponds to $\mathbf{p}^{s'}$, which is a keypoint in the source image. $\mathcal{F}(\mathbf{w}(\mathbf{p}^{s'}), \mathbf{M})$ is the transformation computed at $\mathbf{p}^{s'}$ using (2), where the cluster number is k . We only evaluated the top 60% of keypoint matches that had a small error to reduce the effect

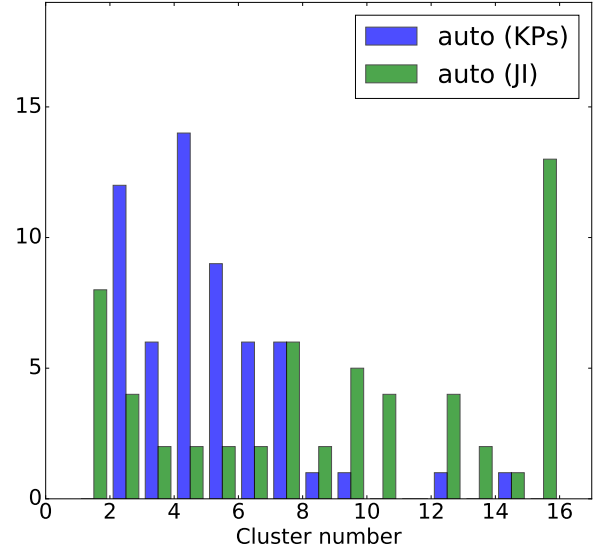


Figure 7. Histogram of the selected cluster number using keypoints (auto (KPs)) and the JI (auto (JI)).

of mismatched keypoints. For each image pair, we increased k while error e_k decreased, then determined the appropriate number of clusters for it.

We applied the algorithm to a part (Fig. 7 and Fig. 8) or all (Fig. 5) of the dataset used in Section III. Fig. 7 shows the histogram of the selected cluster number. We evaluated the registration performance of the cluster number selection methods, as shown in (auto (KPs)) of Fig. 5. We observe that it achieved the best performance among the other methods.

The second method uses the JI of the entire tissue that was extracted in Section II-A as a criterion to evaluate the number of clusters. We evaluated the JI for $k = [1, 16]$ using the brute-force approach, and selected the best JI for each image pair. Fig. 7 shows the histogram of the cluster number with the best JI, in addition to the above.

To compare the performance of these methods, we use two criteria: the JI of the entire tissue and JI of the manually annotated region of the central nervous system. Because the second method maximizes the JI of the entire tissue using the brute-force approach, it must be the best result under the first criterion. The second criterion is blind for both two methods; thus, it provides a fair and solid comparison because the manually annotated region is considered to be correct. As a result, the method using keypoints is comparable to the best JI method in both the entire and annotated regions (Fig. 8). Note that the method using keypoints has much less computational cost than that using the JI because these methods require the blending of the transformations only at keypoints and at all pixels, respectively. These results support the fact that the method using keypoint matches is efficient and sufficiently appropriate to tune the number of clusters.

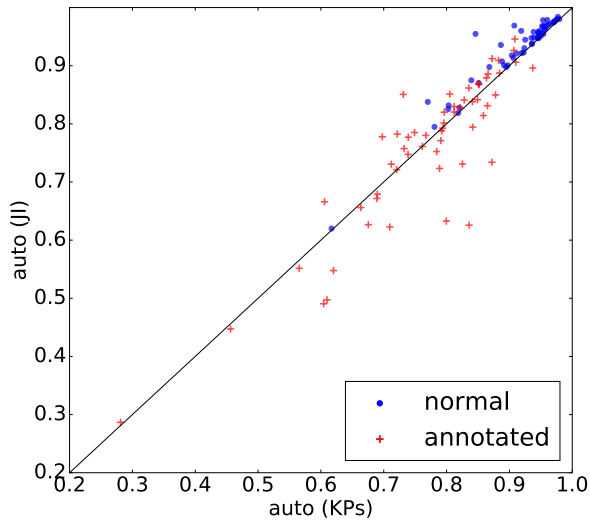


Figure 8. Accuracy comparison of the cluster number selecting method using the keypoints and JI for the same image pair. The x -axis shows the JI of the method using keypoints. The y -axis shows the JI of the method using the JI in each sample. The JIs for the normal and annotated images are shown.

V. CONCLUSION AND FUTURE WORK

In this paper, we proposed a novel feature-based non-rigid registration method that established the transformation field. The proposed method estimated the rigid transformation in local regions and blended them to interpolate the transformations at every pixel. Our method can describe a very complex deformation with a smaller number of control points. We also presented a method to determine the number of local regions automatically. The experiments showed that our method is more robust to staining variation compared with an existing method. However, as a limitation of the feature-based approach, the proposed method could not perform registration in the image without a sufficient number of feature points. This method may have applications other than the registration of histological serial section images. The investigation of other applications of the method will be interesting for future study.

ACKNOWLEDGMENT

This work was partially supported by JSPS KAKENHI Grant Numbers JP15H01121, 15K08134, 17H05296,

26220004 and 26700013.

REFERENCES

- [1] P. F. Alcantarilla, J. Nuevo, and A. Bartoli. Fast Explicit Diffusion for Accelerated Features in Nonlinear Scale Spaces. *Proceedings of the British Machine Vision Conference*, pages 13.1–13.11, 2013. 3
- [2] I. Arganda-Carreras, C. O. S. Sorzano, R. Marabini, J. M. Carazo, C. Ortiz-de Solorzano, and J. Kybic. Consistent and elastic registration of histological sections using vector-spline regularization. *Computer Vision Approaches to Medical Image Analysis*, pages 85–95, 2006. 1, 4
- [3] V. Arsigny, O. Commowick, X. Pennec, and N. Ayache. A Fast and Log-Euclidean Polyaffine Framework for Locally Affine Registration. *Journal of Mathematical Imaging and Vision*, 33(2):222–238, 2006. 1, 2
- [4] V. Arsigny, X. Pennec, and N. Ayache. Polyrigid and Polyaffine Transformations : a Novel Geometrical Tool to Deal with Non-Rigid Deformations . Application to the registration of histological slices. *Medical image analysis*, 9(July):507–523, 2004. 1, 2
- [5] M. A. Fischler and R. C. Bolles. Paradigm for Model. *Communications of the ACM*, 24(6):381–395, 1981. 3
- [6] J. Flusser and B. Zitova. Image registration methods : a survey. *Image and vision computing*, 21:977–1000, 2003. 1
- [7] L. Kavan, S. Collins, J. Zára, and C. O’Sullivan. Geometric skinning with approximate dual quaternion blending. *ACM Transactions on Graphics*, 27:1–23, 2008. 2, 3
- [8] G. Matsuda, S. Kaji, and H. Ochiai. Anti-commutative Dual Complex Numbers and 2D Rigid Transformation. *Mathematical Progress in Expressive Image Synthesis I*, pages 131–138, 2014. 3
- [9] T. Rohlfing. Image similarity and tissue overlaps as surrogates for image registration accuracy: Widely used but unreliable. *IEEE Transactions on Medical Imaging*, 31(2):153–163, 2012. 4
- [10] D. Rueckert, P. Aljabar, R. A. Heckemann, J. V. Hajnal, and A. Hammers. Diffeomorphic registration using B-splines. *Medical image computing and computer-assisted intervention—MICCAI 2006*, 9(2):702–9, 2006. 1
- [11] D. Sheppard. A two-dimensional interpolation function for irregularly-spaced data. *In 23rd National Conference of the ACM*, pages 517–524, 1968. 2
- [12] A. Sotiras, C. Davatzikos, and P. Nikos. Deformable medical image registration: A survey. *IEEE transactions on medical imaging*, 32(7):1153–1190, 2014. 1
- [13] C. Wang, E. B. Gosno, and Y. Li. Fully automatic and robust 3D registration of serial-section microscopic images. *Scientific Reports*, pages 1–14, 2015. 1
- [14] S. Yamada, C. Uwabe, S. Fujii, and K. Shiota. Phenotypic variability in human embryonic holoprosencephaly in the kyoto collection. *Birth Defects Research Part A: Clinical and Molecular Teratology*, 70(8):495–508, 2004. 4